Check for updates

In situ monitoring of functional activity of extracellular matrix stiffness-dependent multidrug resistance protein 1 using scanning electrochemical microscopy†

Shuake Kuermanbayi,‡[ab] Yaowei Yang,‡[ab] Yuxiang Zhao,[ab] Yabei Li,[bc] Le Wang,[d] Jin Yang,[d] Yan Zhou,[ab] Feng Xu [ID] *[ab] and Fei Li [ID] *[ab]

Extracellular matrix (ECM) stiffness affects the drug resistance behavior of cancer cells, while multidrug resistance protein 1 (MRP1) on the cell membrane confers treatment resistance *via* actively transporting drugs out of cancer cells. However, the relationship between ECM stiffness and MRP1 functional activity in cancer cells remains elusive, mainly due to the technical challenge of *in situ* monitoring. Herein, we engineered *in vitro* cancer cell models using breast cancer cells (MCF-7 and MDA-MB-231 cells) as the reprehensive cells on polyacrylamide (PA) gels with three stiffness, mimicking different developmental stages of cancer. We *in situ* characterized the functional activity of MRP1 and investigated the effect of ECM stiffness on MRP1 of cancer cells before and after vincristine treatment using scanning electrochemical microscopy (SECM) with ferrocenecarboxylic acid (FcCOOH) as the redox mediator and endogenous glutathione (GSH) as the indicator. The SECM results show that the functional activity of MRP1 is enhanced with increasing ECM stiffness, and the MRP1-mediated vincristine efflux activity of MCF-7 cells is more affected by ECM stiffness than that of MDA-MB-231 cells. This work, for the first time, applied SECM to *in situ* and quantitatively monitor the functional activity of MRP1 in cancer cells in different tumor mechanical microenvironments, which could help to elucidate the mechanism of matrix stiffness-dependent drug resistance behavior in cancer cells.

Introduction

Cancer is a leading cause of death in the world,[1] and resistance to chemotherapy is one key factor limiting cure in cancer therapy.[2,3] On the one hand, decreased chemotherapeutic drug sensitivity of cancer cells has been proven to be closely related to multidrug resistance proteins (MRPs), which are part of the ATP-binding cassette transporters of the transmembrane protein family and actively remove drugs from cancer cells employing energy derived from ATP hydrolysis.[4,5] For instance, MRPs are proven to be highly expressed in breast, ovarian and lung cancer cells.[6–8] Multidrug resistance-associated protein 1 (MRP1), one of the important MRPs, can recognize and expel therapeutic drugs, leading to decreased drug accumulation in cancer cells (*i.e.*, chemotherapy resistance).[9] Previous studies have shown that MRP1 is localized on lipid rafts of the cell plasma membrane and functions as an efflux pump stabilized by cortical actin;[10] thus, the lipid environment of cell membranes affects the optimal function of MRP1. On the other hand, increased extracellular matrix (ECM) stiffness has been recently recognized as a key hallmark of cancer, due to its effect on accelerating tumor progression, reducing the cure ratio and promoting chemotherapeutic resistance of cancer cells.[11–14] For example, the drug resistance of breast cancer cells increases with increasing matrix stiffness by impeding drug delivery ability and reducing cell sensitivity to drugs.[15–20] And the ECM stiffness can regulate the cytoskeleton to affect cell membrane tension,[21,22] which may also affect the functional activity of MRP1. Therefore, to better understand ECM stiffness-dependent drug resistance, it is of great importance to clarify the effect of ECM stiffness on the functional activity of MRP1 in cancer cells.

Some previous studies have demonstrated that the expression of MRP1 is correlated with poor clinical outcomes in cancer, while others have not observed this correlation.[23] The

[a] The Key Laboratory of Biomedical Information Engineering of Ministry of Education, School of Life Science and Technology, Xi'an Jiaotong University, 710049, Xi'an, Shaanxi, China. E-mail: fengxu@mail.xjtu.edu.cn; feili@mail.xjtu.edu.cn

[b] Bioinspired Engineering and Biomechanics Center (BEBC), Xi'an Jiaotong University, 710049, Xi'an, Shaanxi, China

[c] School of Chemistry, Xi'an Jiaotong University, 710049, Xi'an, Shaanxi, China

[d] Department of Oncology, The First Affiliated Hospital of Medical College, Xi'an Jiaotong University, 710049, Xi'an, Shaanxi, China

† Electronic supplementary information (ESI) available. See https://doi.org/10.1039/d2sc02708a

‡ These authors contributed equally to this work.

difference can be related to the fact that the expression of MRP1 does not always correlate with the functional activity of MRP1, which represents a key index to indicate the cancer cell response to chemotherapeutic treatment.[24] That is, to study cancer cell resistance to chemotherapy, the functional activity of MRP1 offers advantages over its expression.[25] However, the traditional fluorescence method for MRP1 characterization mainly focuses on the expression of MRP1 rather than the functional activity of MRP1, and it remains technically challenging to characterize the functional activity of MRP1 since the viability and function of cancer cells must be maintained during measurement.[24,26] Scanning electrochemical microscopy (SECM), using a microelectrode as its probe to record the currents of redox mediators across the cell surface, can monitor various redox processes across the cell membrane *in situ*.[27–30] The high temporal and spatial resolution, and *in situ* and non-invasive imaging capabilities make it an important analytical tool for living cell analysis.[6,31–36] Moreover, glutathione (*r*-glutamyl cysteingl glycine, GSH), an important intracellular antioxidant for maintaining cellular redox homeostasis, can be transported by MRP1 and is required for several anticancer drugs (*e.g.*, vincristine, doxorubicin and mitoxantrone) transported by MRP1.[37] By recording the redox reaction between the redox mediator (*e.g.*, ferrocenemethanol (FcCH$_2$OH)) in solution and GSH released from cells, SECM can characterize the functional activity of MRP1 in cancer cells.[24,26,38] But FcCH$_2$OH used in the previous SECM studies would diffuse across the cell membrane to promote the intracellular production of GSH,[26,30] which may interfere with the evaluation of functional activity of MRP1 of cancer cells under their normal physiological conditions. Therefore, SECM with an appropriate redox mediator can be an ideal technique for *in situ* monitoring the functional activity of MRP1 of cancer cells and investigating the influence of ECM stiffness on the functional activity of MRP1, which has not been reported yet.

Herein, we engineered *in vitro* cancer cell models using two typical types of breast cancer cells (MCF-7 and MDA-MB-231 cells) as the cancer cell representatives and polyacrylamide (PA) gels with three stiffness to mimic the different developmental stages of breast cancer (Scheme 1a). We evaluated three commonly used redox mediators (*i.e.*, [Ru(NH$_3$)$_6$]Cl$_3$, ferrocenecarboxylic acid (FcCOOH), and FcCH$_2$OH) of SECM experiments, among which FcCOOH was proven to be the appropriate redox mediator for our SECM system. Then we used SECM to investigate the influence of ECM stiffness on the functional activity of MRP1 in breast cancer cells by recording the redox reaction between FcCOOH and the cell-released GSH before and after vincristine (VCR) treatment (Scheme 1b). We quantified the functional activity of MRP1 by the regeneration rate (k) of FcCOOH by the cell-released GSH, which was obtained by simulating the recorded SECM approach curves with the theoretical ones. And we also used calcein acetoxymethyl ester (calcein-AM) and vincristine (VCR), two MRP1 substrates, to confirm the influence of ECM stiffness on the functional activity of MRP1, and performed the immunofluorescence staining, western blot and qRT-PCR analyses to clarify the relationship between MRP1 expression and functional activity. Finally, we compared the MRP1-mediated VCR efflux activity of MCF-7 and MDA-MB-231 cells. This work applied SECM to investigate the relationship between the ECM stiffness and the functional activity of MRP1 in cancer cells *in situ* for the first time, which can offer a better comprehension of the mechanism of ECM stiffness-dependent drug resistance behavior in cancer cells.

Results and discussion

PA gels with three stiffness to mimic ECM stiffness of breast cancer at three pathological stages

According to previous studies,[39–42] the pathological tissue of breast cancer becomes progressively stiffer with the development of breast cancer. In this work, we prepared PA gels with tuneable stiffness by changing the ratios of acrylamide(%) and *N,N'*-methylene-bis-acrylamide (%).[43] The values of Young's moduli of the obtained PA gels measured by using

Scheme 1 Schematic diagram of the assessment of MRP1 functional activity of breast cancer cells (MCF-7 and MDA-MB-231 cells) on PA gels with three stiffness using SECM. (a) Culturing MCF-7 or MDA-MB-231 cells on PA gels with three stiffness to mimic different stages of breast cancer. (b) Illustration of the use of SECM to investigate the functional activity of MRP1 in breast cancer cells cultured on PA gels using FcCOOH as a redox mediator and GSH as an indicator before and after vincristine (VCR) treatment.

a nanoindenter were 2.5 ± 0.7 kPa, 17.1 ± 0.4 kPa and 26.2 ± 0.5 kPa, respectively (Fig. S1, ESI†), which could mimic the stiffness of benign, malignant and advanced stages of breast tumors. The PA gels with three stiffness were then used as the culture substrates for MCF-7 and MB-MDA-231 cells to mimic the *in vitro* ECM mechanical microenvironment of breast cancer.

Investigation of the ECM stiffness effect on the functional activity of MRP1 in cancer cells using SECM

Selection of a redox mediator for the SECM system. To study the effect of ECM stiffness on the functional activity of MRP1, extracellular GSH was chosen as an indicator of MRP1 owing to its role as an endogenous cellular substrate of MRP1,[9] and SECM was employed to record the redox process between extracellular GSH and the redox mediator in solution. To guarantee the ECM stiffness as the only affecter on the functional activity of MRP1 in this case, the redox mediator used in the SECM system is vital which should have a redox reaction with extracellular GSH and cannot permeate the cell membrane to react with the intracellular GSH. Thus, we first evaluated the three commonly used redox mediators in previous SECM reports, *i.e.*, $[Ru(NH_3)_6]Cl_3$, FcCOOH and $FcCH_2OH$, by using them as the redox mediators in our SECM system to image the breast cancer cells (MCF-7) cultured on a 2.5 kPa PA gel (Fig. 1a). As shown in Fig. 1b, since $[Ru(NH_3)_6]Cl_3$ is cell-impermeable and cannot interact with GSH,[26] the normalized probe current decreases from 1 to 0.4 when the probe approaches the cell surface, which can be due to the hindering effect of MCF-7 cells on $[Ru(NH_3)_6]Cl_3$ diffusion to the probe. Thus, the SECM probe current in this case only reflects the topography of MCF-7 cells, consistent with the previous report.[24] As shown in Fig. 1c, since FcCOOH is cell-impermeable,[35] the normalized probe current decreases from 1 to 0.65 when the probe approaches the cell surface, which is because FcCOOH cannot diffuse through the cell membrane, and thus, its diffusion towards the probe is hindered. But owing to the redox reaction between the probe oxidized $[FcCOOH]^+$ and the cell-released GSH at the cell surface, the obtained normalized probe current decreases less than that of $[Ru(NH_3)_6]Cl_3$. Thus, the cell topography and the regeneration reaction of FcCOOH both affect the SECM probe current in this case, consistent with our previous reports.[27,28] As shown in Fig. 1d, when using $FcCH_2OH$ as the redox mediator,

the normalized probe current decreases from 1 to 0.79 when the probe approaches the cell surface, which can be due to the hindering effect of MCF-7 cells on the diffusion of $FcCH_2OH$ towards the probe. And since $FcCH_2OH$ is cell-permeable and can promote the release of GSH from cells,[26] which is involved in the redox cycle of $FcCH_2OH/[FcCH_2OH]^+$, it leads to a higher approaching current compared to that of using FcCOOH as the redox mediator when the probe approaches to the cell surface. It may interfere with the SECM characterization of the functional activity of MRP1 when considering the substrate stiffness as the only affecter. Based on these results, we thus selected FcCOOH, which can interact with the cell-released GSH and also is cell-impermeable, as the redox mediator of the SECM system to characterize the functional activity of MRP1 of breast cancer cells on PA gels, in this case.

Then, as shown in Scheme 1b, in our SECM system, FcCOOH is oxidized to $[FcCOOH]^+$ at the SECM probe surface applied with a potential of 0.5 V (*vs.* Ag/AgCl RE) (eqn (1)). When the probe approaches the cell surface, the cell-released GSH, which is transported by MRP1 at the cell membrane, reduces the probe-oxidized $[FcCOOH]^+$ back to FcCOOH (eqn (2)), leading to an enhanced flux of FcCOOH towards the probe surface and thus an increased oxidation current at the SECM probe.[27,28]

$$FcCOOH \rightarrow [FcCOOH]^+ + e^- \text{ (SECM probe surface)} \quad (1)$$

$$2[FcCOOH]^+ + 2GSH \rightarrow 2FcCOOH + GSSG \text{ (cell surface) } (2)$$

To extract the regeneration rate (k) of FcCOOH by the cell-released GSH at the cell surface, a two-dimensional axially symmetric theoretical model of the SECM experimental system was developed using COMSOL Multiphysics software following the previously reported method (Fig. S2, ESI†).[28] The theoretical models considering the average cell heights and average diameters of the MCF-7 and MDA-MB-231 cells on the PA gels at each stiffness were built and used in the simulation. The k value is related to the GSH efflux rate and represents the functional activity of MRP1, and it can be obtained by simulating the recorded experimental approach curves of SECM with the theoretical curves. The detailed reaction process, determination of the highest point of the cell, and parameters (including cell topography, probe-cell surface distance, *etc.*) used in the simulation were determined by the methods described in the

Fig. 1 (a) Optical microscope image and (b–d) the corresponding SECM images of a single MCF-7 cell cultured on the PA gel with a stiffness of 2.5 kPa using different redox mediators. (b) 0.5 mM $[Ru(NH_3)_6]Cl_3$ ($E_{probe} = -0.35$ V *vs.* Ag/AgCl RE), (c) 0.5 mM FcCOOH ($E_{probe} = 0.5$ V *vs.* Ag/AgCl RE), and (d) 0.5 mM $FcCH_2OH$ ($E_{probe} = 0.5$ V *vs.* Ag/AgCl RE). The probe/cell distances were set to 5 μm for SECM 2D scanning experiments. All the SECM measurements were performed using a 10 μm-in-diameter Pt microelectrode as the SECM probe.

Experimental section and are shown in Fig. S2–S5 and Table S1 (ESI†).

ECM stiffness-dependent functional activity of MRP1 in cancer cells characterized by SECM. As shown in Fig. 2a and b, when the SECM probe approaches the surfaces of MCF-7 and MDA-MB-231 cells on the stiff PA gels (17.1 and 26.2 kPa), the SECM probe currents become higher compared to the cell surfaces on the soft PA gels (2.5 kPa). This could be because more GSH permeates across the cell membrane and reacts with extracellular $[FcCOOH]^+$, which can compensate for the probe-oxidized FcCOOH resulting in an increased probe current. However, since the GSH released from cells cannot replenish the overall probe-oxidized FcCOOH, the approach curves of the cells still exhibit a negative feedback trend. By simulating the experimental approach curves with the theoretical curves, we obtained the average k values of MCF-7 and MDA-MB-231 cells on the PA gels with three stiffness (Fig. 2c and d), in which the k values increase with increasing substrate stiffness for both MCF-7 and MDA-MB-231 cells, demonstrating that a stiffer ECM could enhance the extracellular GSH levels of both cell types.

To verify whether the increased extracellular GSH level is related to the efflux of intracellular GSH, we also characterized the intracellular GSH levels by the fluorescence method (Fig. 3). We can observe that the intracellular GSH levels in both cell types decrease with increasing ECM stiffness, which can be related to multiple factors and efflux of GSH can be one of the

important factors.[44] From the results, it can be speculated that ECM stiffness may alter the GSH efflux ability of breast cancer cells. Since GSH can be actively transported out of cells by MRP1,[9] the changes in the GSH efflux ability of breast cancer cells are thus related to the change in the functional activity of MRP1.

To confirm that the changes in the GSH efflux abilities of the breast cancer cells are dependent on the activity of MRP1, MK571 (a known MRP1 inhibitor[6]) was added to the cell culture and used to perform the inhibiting MRP1 experiments. The SECM experimental and the theoretical approach curves of the MCF-7 and MDA-MB-231 cells after the MK571 treatment are shown in Fig. 4a and b, from which we can see that all the k values of the MCF-7 and MDA-MB-231 cells with the MK571 treatment are smaller than those without the MK571 treatment on the PA gels with the same stiffness (Fig. 2a and b). It can be because in the presence of MK571, the efflux of intracellular GSH decreases, indicating that the inhibition of activity of MRP1 decreases the efflux of GSH. Therefore, the results confirm that the changes in the GSH efflux abilities of the breast cancer cells are indeed dependent on the activities of MRP1. The statistical results of the average k values of the MCF-7 cells and MDA-MB-231 cells on the PA gels with three stiffness are shown in Fig. 4c and d. From Fig. 4c, we can observe that there is no significant difference in the k values of the MCF-7 cells on the PA gels with different stiffnesses, indicating that the efflux
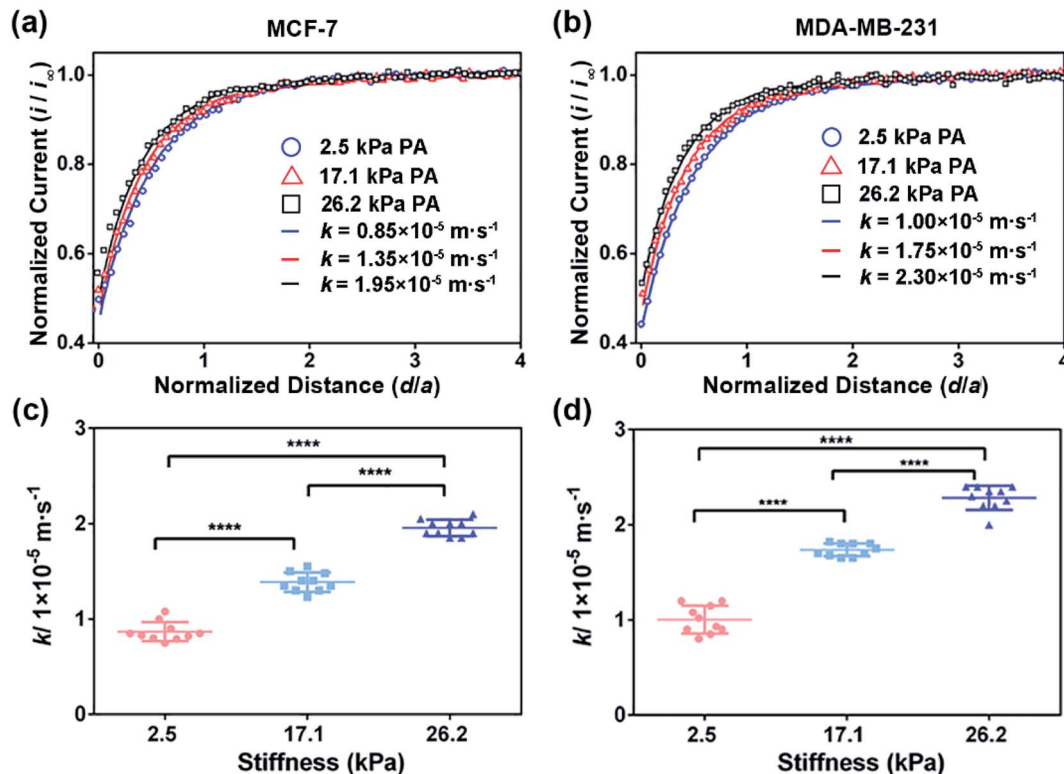

Fig. 2 SECM approach curves of (a) MCF-7 cells and (b) MDA-MB-231 cells cultured on the PA gels with stiffness of 2.5, 17.1 and 26.2 kPa, respectively. Statistical results of the average k values of (c) MCF-7 cells ($n = 9$) and (d) MDA-MB-231 cells ($n = 9$) on the PA gels with different stiffness. Data are shown as the mean $\pm$ sd. ****$p < 0.0001$ (one-way ANOVA). All the SECM measurements were performed using a 10 μm-in-diameter Pt microelectrode as the SECM probe.
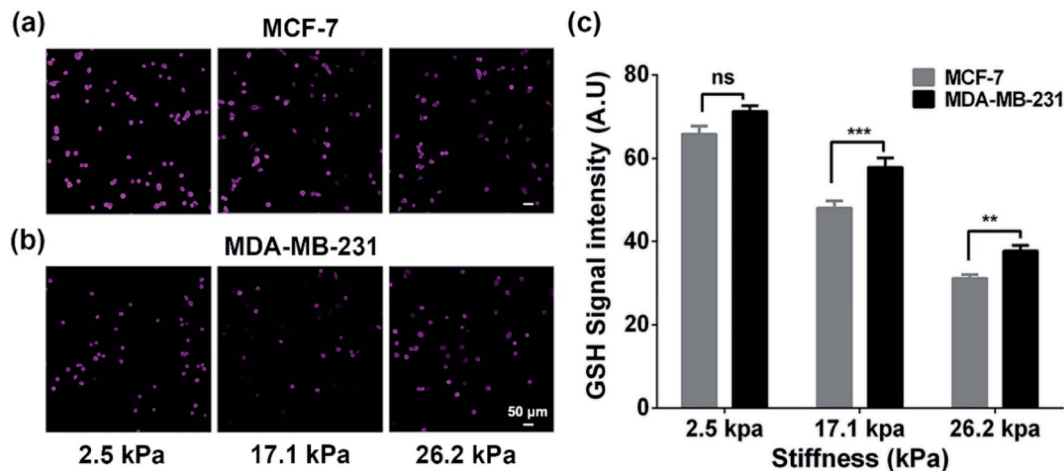
Fig. 3 (a and b) Fluorescence images and (c) intensities of the intracellular GSH concentrations of (a) MCF cells and (b) MDA-MB-231 cells on the PA gels with stiffness of 2.5, 17.1, and 26.2 kPa, respectively (scale bar: 50 μm). Data are shown as the mean ± sd. **$p < 0.01$ and ***$p < 0.001$ (one-way ANOVA).
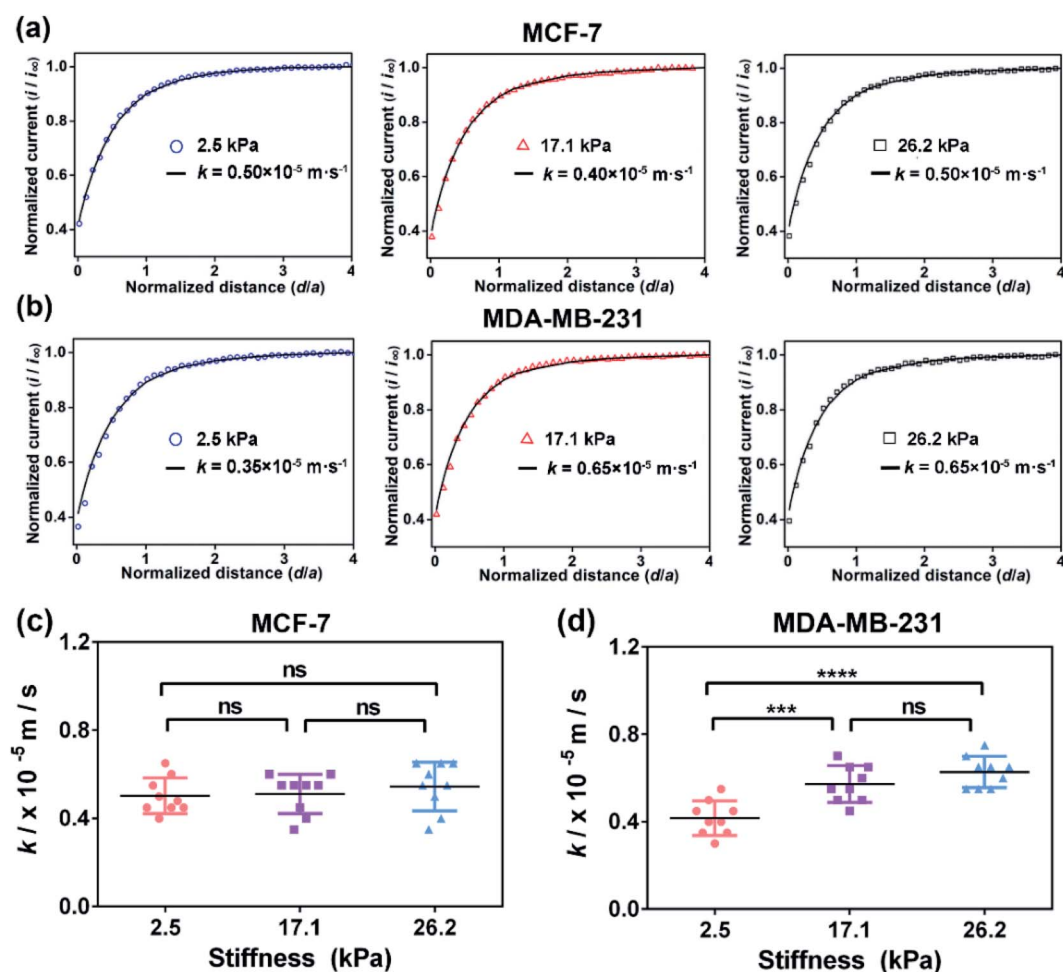

Fig. 4 SECM approach curves of (a) the MCF-7 cells and (b) the MDA-MB-231 cells on the PA gels with stiffness of 2.5, 17.1 and 26.2 kPa, respectively, after the MK571 treatment. Statistical results of the average k values of (c) MCF-7 cells ($n = 9$) and (d) MDA-MB-231 cells ($n = 9$) on the PA gels with different stiffness. Data are shown as the mean ± sd. ***$p < 0.001$ and ****$p < 0.0001$ (one-way ANOVA).

ability of MRP1 of the MCF-7 cells is inhibited to a similar extent on the PA gels with different stiffness. From Fig. 4d, we can see that the k values of the MDA-MB-231 cells on the stiff PA gels (17.1 and 26.2 kPa) are higher compared to those on the soft PA gels (2.5 kPa), indicating that the efflux ability of MRP1 of the MDA-MB-231 cells on the soft PA gels is inhibited to a greater extent than those on the stiff PA gels. It further demonstrates that the ECM stiffness may affect the inhibitory effect of MK571 on the functional activity of MRP1 of MDA-MB-231 cells. Collectively, all these results demonstrate that the increased ECM stiffness enhances the functional activity of MRP1 in MCF-7 and MDA-MB-231 cells.

Investigation of the ECM stiffness effect on the expressions and the functional activity of MRP1 in cancer cells

To explore whether the enhanced functional activity of MRP1 in breast cancer cells with increasing substrate stiffness is caused by the enhanced MRP1 expression on the cell membrane, we also characterized the expressions of MRP1 in MCF-7 and MDA-MB-231 cells using the immunofluorescence staining method.

We can see that there is no significant difference in the immunofluorescence images of MCF-7 and MDA-MB-231 cells on the PA gels with three stiffness (Fig. 5a and b), which is further confirmed by quantitative analysis of the normalized total immunofluorescence intensities (Fig. 5c and d), indicating that the ECM stiffness has no significant influence on the MRP1 expressions of the breast cancer cells. We also performed the western blot experiments to investigate the relationship between the MRP1 expression levels of the MCF-7 cells and MDA-MB-231 cells and the PA gel stiffness. From Fig. 5e, we can observe that the expression levels of MRP1 of the MCF-7 and MDA-MB-231 cells are not affected by the PA gel stiffness, which is similar to the above immunofluorescence staining results shown in Fig. 5a and b. These results further indicate that the ECM stiffness has no significant influence on the MRP1 expressions of the breast cancer cells. Moreover, to check whether the stiffness of PA gels changes the expressions of the mRNA encoding MRP-1 in the MCF-7 and MDA-MB-231 cells on the PA gels with different stiffness in our case, we also performed the qRT-qPCR experiments to analyse the mRNA levels of MRP1 in the two types of cells. From the obtained qRT-qPCR
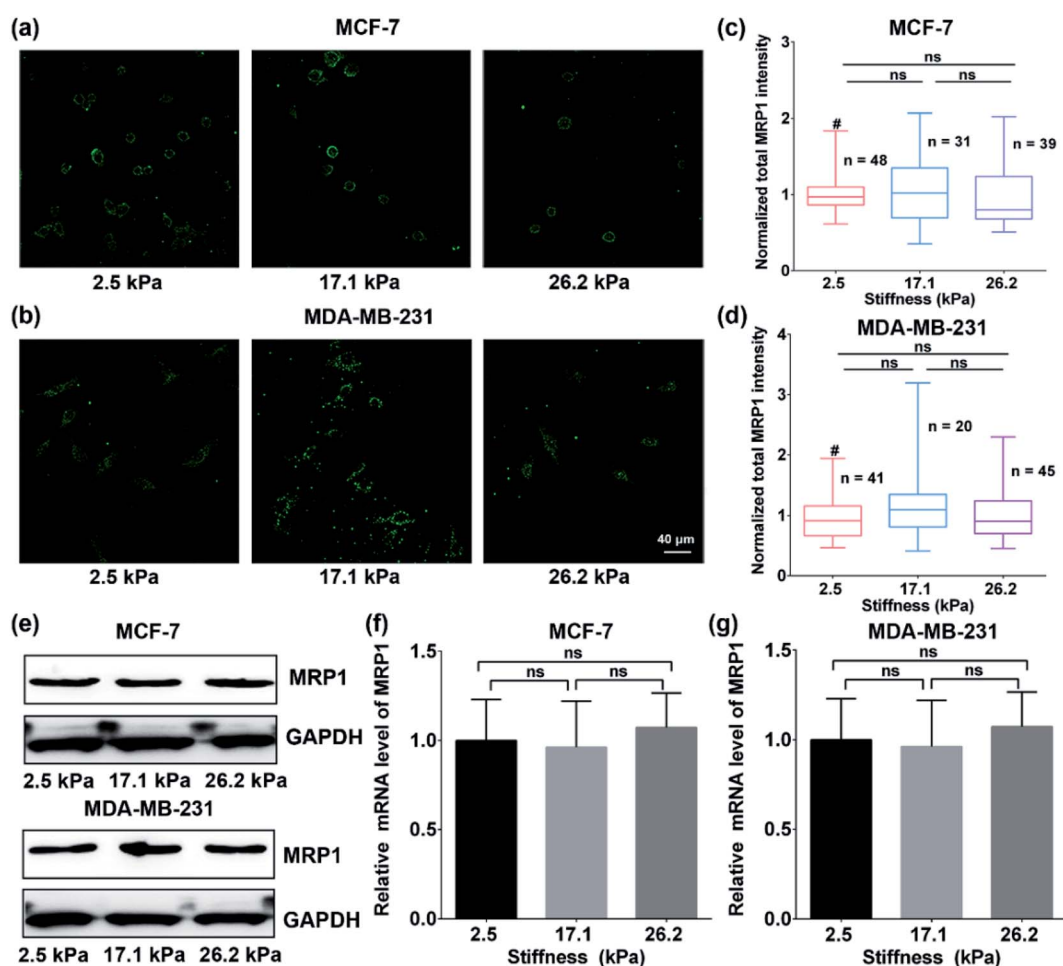

Fig. 5 (a and b) Immunofluorescence images and (c and d) the normalized total MRP1 intensities of (a and c) MCF cells and (b and d) MDA-MB-231 cells on the PA gels with stiffness of 2.5, 17.1 and 26.2 kPa, respectively (scale bar: 40 μm). (e) Western blot analysis of the MRP1 expressions of the MCF-7 and MDA-MB-231 cells on the PA gels with stiffness of 2.5, 17.1 and 26.2 kPa, respectively. (f and g) The relative MRP1 mRNA expressions in (f) the MCF-7 cells and (g) the MDA-MB-231 cells on the PA gels with stiffness of 2.5, 17.1 and 26.2 kPa, respectively.

results shown in Fig. 5f and g, we can see that there is no significant difference in the mRNA levels of MRP1 in both the MCF-7 cells and the MDA-MB-231 cells on the PA gels with three stiffness, indicating that the increased PA gels stiffness does not change the levels of the mRNA encoding MRP1 in the two types of cells. Thus, it can be concluded that the increased ECM stiffness enhances the MRP1 functional activity of MCF-7 and MDA-MB-231 cells without altering their expression on the cell membrane, *i.e.*, the functional activity and expression of MRP1 do not directly correlate, which is consistent with the results of the previous study.[25] A possible reason is that collagen type 1, which is the ECM component, has been proven to have no significant influence on the expression level of MRP1 of MCF-7 cells and almost no influence on the expression level of MRP1 in MDA-MB-231 cells but can increase the functional activity in MRP1 in the two cell lines.[45] Our findings clearly reveal the contribution of ECM stiffness to the functional activity of MRP1 in breast cancer cells, for the first time.

Moreover, to further confirm the effect of ECM stiffness on the functional activity of MRP1 in MCF-7 and MDA-MB-231 cells, we also used fluorescent efflux assay of calcein-AM, a well-known substrate of MRP1,[46] to study the functional activity of MRP1. In the measurements, calcein-AM can be metabolized by cytosolic esterases into hydrophilic and green fluorescent substance-calcein, which can be transported by MRP1. Thus, the changes in the functional activity of MRP1 can be evaluated by the remaining intracellular calcein. The obtained relative amounts of calcein transported by MRP1 of the MCF-7 and MDA-MB-231 cells on the PA gels with 2.5, 17.1 and 26.2 kPa stiffness are 50.34%, 52.51%, and 58.37% (MCF-7), and 22.45%, 32.14%, and 41.65% (MDA-MB-231), respectively (Fig. 6a and b). The results show that the intracellular retention of calcein in both cell types decreases with increasing ECM stiffness, indicating that the increased ECM stiffness enhances the functional activity of MRP1, which is also consistent with the above SECM experimental results.

According to previous studies,[10,47] the function of MRP1, which is located in lipid rafts on the cell membrane, as an efflux pump, depends on cortical actin. Destruction of cortical actin by the MRP1 inhibitor can lead to the weakening efflux activity

of MRP1, which is accompanied by the internalization of partial proteins. The functional activity of MRP1 is mainly related to its localization in lipid rafts rather than its internalization.[10] With the change in ECM stiffness, the mechanical cue regulates the tension of the cell membrane/cortical fiber and affects the intracellular skeleton rearrangement as well as cell morphology and cell volume.[22,48] Therefore, it can be inferred that the enhanced MRP1 functional activity of breast cancer cells on stiffer substrates may be related to the change in cell membrane tension in this case.

Investigation of the effect of ECM stiffness on the MRP1-mediated chemotherapeutic drug efflux activity of cancer cells by SECM

To further explore the effect of ECM stiffness on the drug efflux activity of MRP1 in breast cancer cells, vincristine (VCR), a broad-spectrum cancer chemotherapy drug used for breast cancer treatment in the clinic and an excellent substrate for MRP1,[9,49] was selected as a representative anticancer drug. First, to evaluate the potency of VCR on MCF-7 and MDA-MB-231 cells while maintaining cell viability, the half inhibition concentrations (IC_{50}) of VCR of the two cell types were determined through a cell viability assay, which are 245.0, 620.4, and 1137.0 nM for MCF-7 cells and 163.0, 234.4, and 343.2 nM for MDA-MB-231 cells on PA gels with stiffness of 2.5, 17.1 and 26.2 kPa, respectively (Fig. S6, ESI†). Then, we utilized SECM to assess the effect of ECM stiffness on the efflux activity of MRP1 of VCR of MCF-7 and MDA-MB-231 cells after treatment with IC_{50} doses of VCR. Moreover, considering that the possible change in cell membrane permeability under VCR treatment can lead to the transport of FcCOOH into cells, we also used SECM with $[Ru(NH_3)_6]Cl_3$ as the redox mediator to characterize the membrane permeability of MCF-7 and MDA-MB 231 cells on the 26.2 kPa PA gels with and without VCR treatment. As shown in Fig. S7a and b (ESI†), both MCF-7 and MDA-MB 231 cells after the VCR treatment show a more circular shape than those without VCR treatment, which can be related to VCR binding microtubules to inhibit mitosis.[50] And from the SECM approach curves in Fig. S7c and d (ESI†), we can see that there is no significant difference in the SECM approach curves for both cell
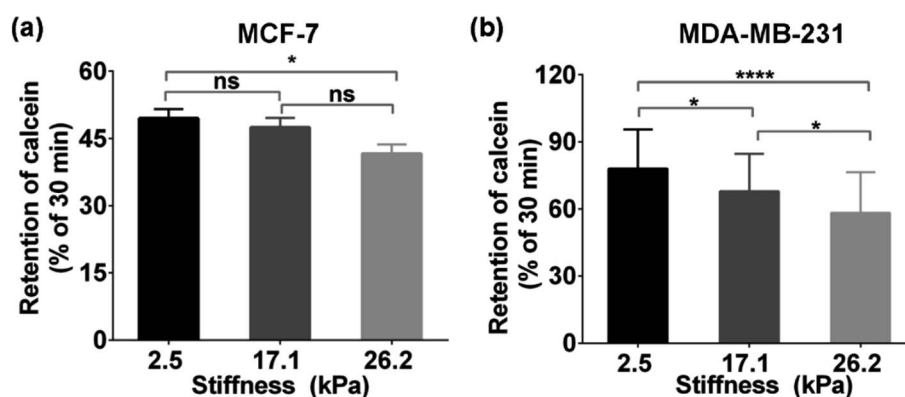

Fig. 6 Intracellular retention calcein (% of 30 min) of (a) MCF-7 cells and (b) MDA-MB-231 cells on the PA gels with stiffness of 2.5, 17.1, and 26.2 kPa, respectively. Data are shown as the mean ± sd. *$p < 0.05$ and ****$p < 0.0001$ (one-way ANOVA).

types before and after VCR treatment, indicating that VCR treatment has nearly no effect on the cell membrane permeability of the two types of breast cancer cells.

Then, we studied the effect of ECM stiffness on the MRP1-mediated VCR efflux activity of MCF-7 and MDA-MB 231 cells by SECM *via* recording the redox process between extracellular FcCOOH in solution and cell-released GSH after VCR treatment. The obtained SECM experimental and simulated theoretical approach curves are shown in Fig. 7a and b. As illustrated in Scheme 1b, in this case, during the process by which breast cancer cells actively transport VCR out of cells, GSH is co-transported with VCR out of cells and thus acted as a cofactor for VCR transport.[51,52] When the probe approaches the cell surface on the PA gel, GSH could be co-transported with VCR by MRP1 and then react with the extracellular $[FcCOOH]^+$, which can be compensated by the probe-oxidized FcCOOH and lead to an increase in the probe current. Through simulation of the experimental approach curves with the theoretical curves, the k

values of MCF-7 cells and MDA-MB-231 cells on the PA gels with three stiffness after the VCR treatment were obtained. From Fig. 7c and d, we can see that the k values of MCF-7 and MDA-MB-231 cells increase with increasing ECM stiffness after VCR treatment, indicating that more GSH is transported out of cells with increasing ECM stiffness. This phenomenon can be explained by that a stiffer ECM enhances the functional activity of MRP1; thus, more GSH can be co-transported with VCR. From these results, we can further conclude that breast cancer cells growing on stiffer substrates present enhanced MPR1 functional activity and increased efflux of VCR than those growing on softer substrates.

Comparison of MRP1-mediated VCR efflux abilities of the MCF-7 and MDA-MB-231 cells under different ECM stiffness

MCF-7 (estrogen receptor-positive) and MDA-MB-231 (triple-negative) exhibit phenotypic/genotypic differences and display different response behaviors under anticancer drug treatment.[53]
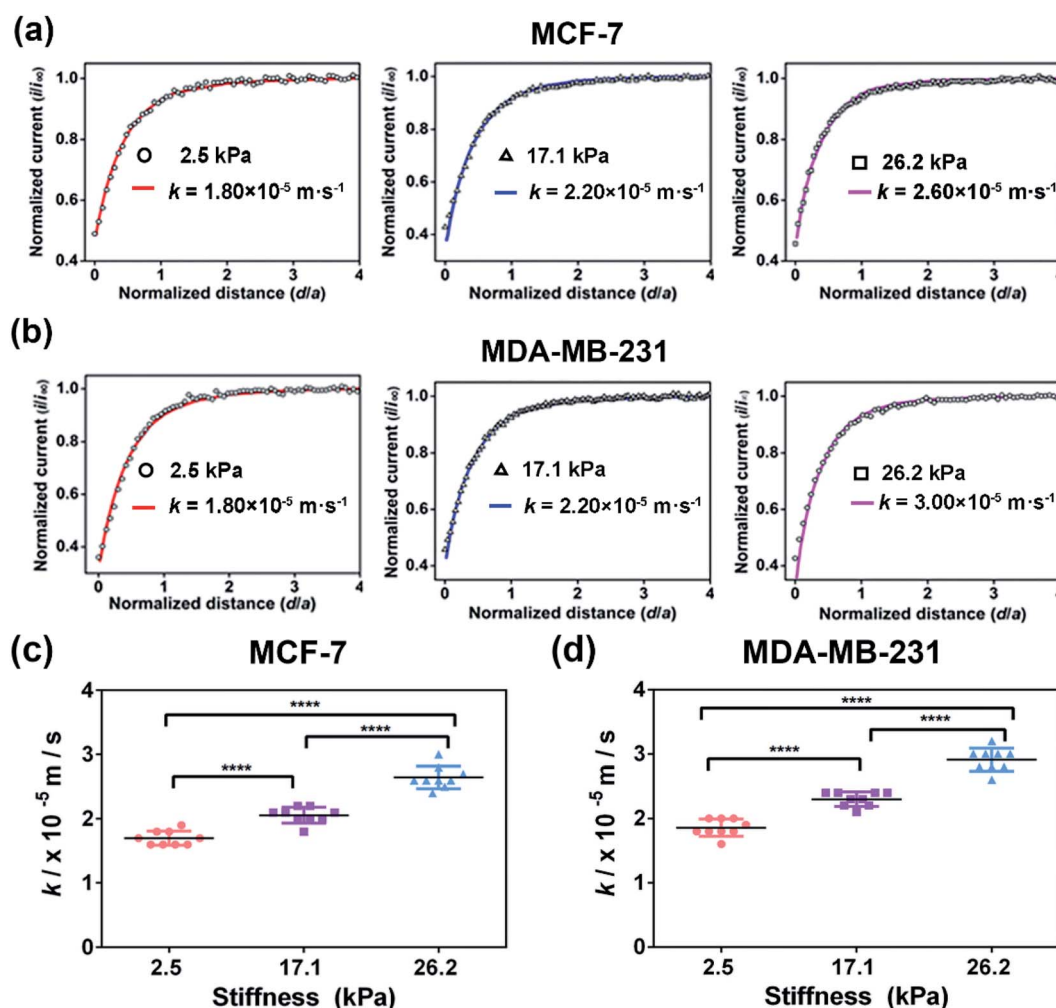

Fig. 7 Assessment of the MRP1 functional activity of MCF-7 and MDA-MB-231 cells cultured on the PA gels with stiffness of 2.5, 17.1 and 26.2 kPa, respectively, after VCR treatment by SECM. SECM approach curves of (a) MCF-7 cells and (b) MDA-MB-231 cells cultured on PA gels with stiffness of 2.5, 17.1 and 26.2 kPa. Statistical results of the average k values of (c) MCF-7 cells ($n = 9$) and (d) MDA-MB-231 cells ($n = 9$) on PA gels with different stiffness. Data are shown as the mean ± sd. ****$p < 0.0001$ (one-way ANOVA). All the SECM measurements were performed using a 10 μm-in-diameter Pt microelectrode as the SECM probe.

Fig. 8 Comparison of the MRP1 functional activity of MCF-7 and MDA-MB-231 cells with/without VCR treatment on the PA gels with stiffness of 2.5, 17.1 and 26.2 kPa, respectively.

To evaluate whether ECM stiffness has different effects on the MRP1-mediated VCR efflux ability of MCF-7 and MDA-MB-231 cells, the k values of the two types of breast cancer cells with or without VCR treatment were compared (Fig. 8). We can observe that all the k values increase with increasing ECM stiffness, and the k values of MCF-7 cells are smaller than those of MDA-MB-231 cells with or without VCR treatment on PA gels with the same stiffness.

To better compare the MRP1-mediated VCR efflux ability, the obtained k values after the VCR treatment were normalized by the k values without the VCR treatment, which is expressed as R ($k_{with\ VCR}/k_{w/o\ VCR}$). From Table 1, it can be seen that the values of MCF-7 cells are higher than those of MDA-MB-231 cells on PA gels with three stiffness after the VCR treatment, indicating that the ECM stiffness has a greater effect on the VCR efflux activity of MCF-7 cells than on that of MDA-MB-231 cells. Meanwhile, from the dose–response curves in Fig. S6 (ESI†), we can see that the IC_{50} values of VCR for MCF-7 and MDA-MB-231 cells increase with increased ECM stiffness, demonstrating that both MCF-7 and MDA-MB-231 cells are less sensitive to VCR with increasing ECM stiffness. Additionally, the IC_{50} values of VCR for MCF-7 cells are higher than those of MDA-MB-231 cells on the PA gels with the same stiffness, indicating that the MCF-7 cells are less sensitive to VCR than the MDA-MB-231 cells, which could be related to the greater VCR efflux ability of the MCF-7 cells. All these results prove that ECM stiffness has different effects on the VCR efflux activity of different subtypes of breast cancer cells, indicating the significant role of ECM stiffness in the chemotherapy resistance of breast cancer.

Conclusions

In this work, we engineered *in vitro* cancer cell models by mimicking the benign, malignant and advanced stages of breast cancer using PA gels with stiffness of 2.5 ± 0.7 kPa, 17.1 ± 0.4 kPa and 26.2 ± 0.5 kPa, respectively, and MCF-7 and MDA-MB-231 cells as the representative breast cancer cells. SECM was employed to *in situ* and quantitatively assess the effect of ECM stiffness on the functional activity of MRP1 in the two types of cancer cells using FcCOOH as the redox mediator and endogenous GSH as the indicator. The SECM results show that the regeneration rate (k) of FcCOOH by the cell-released GSH increases with increasing ECM stiffness, indicating that increasing ECM stiffness can enhance the functional activity of MRP1. And the immunofluorescence staining, western blot and qRT-PCR analysis results confirm that the altered functional activity of MRP1 is not caused by the alteration of MRP1 expression. The k values increase with increasing ECM stiffness after VCR treatment, further proving the increased MRP-mediated VCR efflux ability with increased ECM stiffness. From the comparison result of $k_{with\ VCR}/k_{w/o\ VCR}$ of the two breast cancer cells, the ECM stiffness shows a greater effect on the VCR efflux activity of MCF-7 cells than MDA-MB-231 cells, and MCF-7 cells present stronger efflux ability to VCR than MDA-MB-231 cells. This work used the SECM approach to *in situ* investigate the functional activity of MRP1 in cancer cells under different ECM stiffnesses for the first time. The findings are important as they provide a better understanding of the effect of a mechanical factor of the cell microenvironment on the drug resistance behavior of cancer cells. Further exploring the potential regulatory mechanisms may help in deriving therapeutic targets.

Experimental

SECM measurements

All SECM experiments were done using a SECM instrument (ElProScan 3, HEKA Elektronik GmbH, Harvard Bioscience Inc.) in combination with an inverted optical microscope (Nikon, TS100-F, Japan). A three-electrode system was employed in all the SECM experiments, in which the SECM probe/working electrode was a 10 μm-in-diameter Pt ultramicroelectrode (UME, RG = 2), the reference electrode was a 0.6 mm-in-diameter Ag/AgCl wire and the counter electrode was a 0.5 mm-in-diameter Pt wire.

Before the SECM experiments, MCF-7 cells and MDA-MB-231 cells were seeded at a density of 1×10^4 cells cm^{-2} on the PA gels with different stiffness and then cultured in an incubator (5% CO$_2$, 37 °C). After 24 hours, the cell medium containing MCF-7 or MDA-MB-231 cells was replenished with an L-15 medium containing 0.5 mM FcCOOH and equilibrated for 10 minutes. Then, the probe, which was applied with the oxidation

Table 1 The R values of MCF-7 and MDA-MB-231 cells on the PA gels with three stiffness

Cancer cell	Stiffness (kPa)	R values
MCF-7	2.5 ± 0.7	2.0
	17.1 ± 0.4	1.5
	26.2 ± 0.5	1.3
MDA-MB-231	2.5 ± 0.7	1.8
	17.1 ± 0.4	1.3
	26.2 ± 0.5	1.2

potential of FcCOOH (0.5 V *vs.* Ag/AgCl RE), was firstly approached to the PA gel around the cell and then to the cell surface with the aid of the inverted microscope. When the tip of the SECM probe touched the PA gel surface or the cell surface, which can also be observed by the inverted optical microscope combined with the SECM system, an "inflection" point of the probe current-distance curve was obtained, which was then regarded as the zero point of the approach curve. And when an "inflection" point appeared in the approach curve, the probe was manually stopped and then lifted up by 25 μm and moved to the top of the cell surface. Subsequently, the probe was lifted up by another 25 μm and approached the cell surface vertically with a velocity of 0.5 μm s^{-1}.

When performing approaching experiments on the cells on the PA gels, first, to determine the "highest point" of the cell on the PA gels, the 2D scan and line scan modes of SECM were used along two perpendicular directions. After the probe approaches the cell surface, the probe was raised up by 5 μm and moved to the edge of the cell in the x and y directions. Then, after determining the scanning area on the cell by observing the cell size using the inverted microscope, 2D SECM scanning on the cells was carried out with a scanning speed of 2 μm s^{-1} and a scanning interval of 1 μm. The highest point of the cell was consequentially determined according to the obtained cell morphology-probe current map. Finally, the probe was raised up by 20 μm and then approached the highest point of the cell in the z-axis to obtain the approach curves.

SECM theoretical model

The simulation model of the SECM experiments was developed in 2D axial symmetry coordinates by COMSOL Multiphysics software 3.5a (COMSOL Inc., Sweden). As illustrated in Fig. S2 (ESI†), the r-axis and z-axis are parallel and perpendicular to the Pt microelectrode (UME) surface, respectively. The origin of the coordinate axes is set at the middle of the Pt UME (5 μm in radius, RG = 2).

The redox reactions occurring at the probe and cell surface are shown in eqn (1) and (2) (see above). The diffusion of FcCOOH at the probe surface follows Fick's law of diffusion, which can be expressed by using eqn (3).

$$\frac{\partial c(r,z,t)}{\partial t} = D\left[\frac{\partial^2 c(r,z,t)}{\partial r^2} + \frac{1}{r}\frac{\partial c(r,z,t)}{\partial r} + \frac{\partial^2 c(r,z,t)}{\partial z^2}\right] = 0 \quad (3)$$

where r and z are the axisymmetric coordinates, t is the time and $c(r,z)$ is the local concentration of FcCOOH. The initial condition of eqn (4) is defined as:

$$c(r,z) = c_0, \, t = 0 \quad (4)$$

The redox reaction at the cell surface is presumed to be an irreversible reaction. Then the regeneration rate constant, k, is simulated and the boundary condition at the cell surface follows eqn (5).

$$D\left[\frac{\partial c(r,z)}{\partial z}\right]_{z=d} = k[c_0 - c(r,d)] \quad (5)$$

where c_0 is the concentration of FcCOOH in the bulk solution, D is the diffusion coefficient of FcCOOH ($D = 5.7 \times 10^{-10}$ m^2 s^{-1} in this case), and d is the distance between the probe and the highest point of the cell.

Under diffusion control, the current on the probe surface could be calculated by using the following equation:

$$i_{T,\infty} = 2\pi nFD \int_0^a r\left(\frac{\partial c(r,z)}{\partial z}\right)\mathrm{d}r \quad (6)$$

where n is the electron transfer number ($n = 1$ in this case), F is Faraday's constant (96 485 C mol L^{-1}), D is the diffusion coefficient of FcCOOH ($D = 5.7 \times 10^{-6}$ cm^2 s^{-1} in this case), and a is the probe tip radius ($a = 5$ μm in this work). The detailed boundary conditions of the SECM model are listed in Table S1, ESI.† All the k values in this work are the average values of over nine experiments.

Data availability

The experimental section (including chemicals and materials, preparation and characterization of PA gels, cell culture and treatment with vincristine (VCR), measurement of intracellular GSH levels, characterization of the functional activity and expression of MRP1 in cells, and measurements of drug-dose response and cell viability of VCR), stiffness of PA gels, the 2D axial SECM geometry simulation model, characterization studies of cell topography and probe-cell surface distances in SECM measurements, measurements of IC$_{50}$ values of VCR of MCF-7 and MDA-MB 231 cells on PA gels, and characterization of the cell membrane permeability of MCF-7 and MDA-MB 231 cells on PA gels with/without VCR treatment by SECM, are all provided in the ESI.†

Author contributions

S. K., Y. W. Y., F. X. and F. L. designed the research; S. K. and Y. W. Y. performed all the experiments; Y. X. Z. helped with the western blot and qRT-PCR experiments; S. K., Y. Y. W. and Y. X. Z. analysed the data; Y. B. L. provided the technical support for the SECM experiments; L. W., J. Y. and Y. Z. gave suggestions on the work; S. K., Y. W. Y., F. X. and F. L. wrote the manuscript.

Conflicts of interest

There are no conflicts to declare.

Acknowledgements

Notes and references

1 H. Sung, J. Ferlay, R. L. Siegel, M. Laversanne, I. Soerjomataram, A. Jemal and F. Bray, *Ca-Cancer J. Clin.*, 2021, **71**, 209–249.

2 N. Kurt Yilmaz and C. A. Schiffer, *Chem. Rev.*, 2021, **121**, 3235–3237.

3 N. Vasan, J. Baselga and D. M. Hyman, *Nature*, 2019, **575**, 299–309.

4 C. Holohan, S. Van Schaeybroeck, D. B. Longley and P. G. Johnston, *Nat. Rev. Cancer*, 2013, **13**, 714–726.

5 R. A. Ward, S. Fawell, N. Floc'h, V. Flemington, D. McKerrecher and P. D. Smith, *Chem. Rev.*, 2021, **121**, 3297–3351.

6 D. Koley and A. J. Bard, *Proc. Natl. Acad. Sci. U. S. A.*, 2012, **109**, 11522–11527.

7 B. G. Peterson, K. W. Tan, B. Osa-Andrews and S. H. Iram, *Pharmacol. Res.*, 2017, **119**, 313–326.

8 J. Q. Wang, Y. Yang, C. Y. Cai, Q. X. Teng, Q. Cui, J. Lin, Y. G. Assaraf and Z. S. Chen, *Drug Resistance Updates*, 2021, **54**, 100743.

9 S. P. C. Cole, *Annu. Rev. Pharmacol. Toxicol.*, 2014, **54**, 95.

10 I. Hummel, K. Klappe, C. Ercan and J. W. Kok, *Mol. Pharmacol.*, 2011, **79**, 229–240.

11 J. Huang, L. Zhang, D. Wan, L. Zhou, S. Zheng, S. Lin and Y. Qiao, *Signal Transduction Targeted Ther.*, 2021, **6**, 153.

12 S. C. Wei, L. Fattet, J. H. Tsai, Y. R. Guo, V. H. Pai, H. E. Majeski, A. C. Chen, R. L. Sah, S. S. Taylor, A. J. Engler and J. Yang, *Nat. Cell Biol.*, 2015, **17**, 678.

13 H. T. Nia, L. L. Munn and R. K. Jain, *Science*, 2020, **370**, eaaz0868.

14 J. C. Tung, J. M. Barnes, S. R. Desai, C. Sistrunk, M. W. Conklin, P. Schedin, K. W. Eliceiri, P. J. Keely, V. L. Seewaldt and V. M. Weaver, *Free Radical Biol. Med.*, 2015, **79**, 269–280.

15 M. H. Joyce, C. Lu, E. R. James, R. Hegab, S. C. Allen, L. J. Suggs and A. Brock, *Front. Oncol.*, 2018, **8**, 337.

16 Y. Li, N. Khuu, E. Prince, H. Tao, N. Zhang, Z. Chen, A. Gevorkian, A. P. McGuigan and E. Kumacheva, *Biomacromolecules*, 2021, **22**, 419–429.

17 S. H. Medina, B. Bush, M. Cam, E. Sevcik, F. W. DelRio, K. Nandy and J. P. Schneider, *Biomaterials*, 2019, **202**, 1–11.

18 P. A. Netti, D. A. Berk, M. A. Swartz, A. J. Grodzinsky and R. K. Jain, *Cancer Res.*, 2000, **60**, 2497–2503.

19 T. V. Nguyen, M. Sleiman, T. Moriarty, W. G. Herrick and S. R. Peyton, *Biomaterials*, 2014, **35**, 5749–5759.

20 X. Qin, X. Y. Lv, P. Li, R. Yang, Q. Xia, Y. Chen, Y. T. Peng, L. Li, S. Li, T. T. Li, Y. Jiang, H. Yang, C. H. Wu, C. Zheng, J. Zhu, F. M. You, H. Wang, J. Chen and Y. Y. Liu, *Biochim. Biophys. Acta, Mol. Basis Dis.*, 2020, **1866**, 165625.

21 M. Guo, A. F. Pegoraro, A. Mao, E. H. Zhou, P. R. Arany, Y. Han, D. T. Burnette, M. H. Jensen, K. E. Kasza, J. R. Moore, F. C. Mackintosh, J. J. Fredberg, D. J. Mooney, J. Lippincott-Schwartz and D. A. Weitz, *Proc. Natl. Acad. Sci. U. S. A.*, 2017, **114**, E8618–E8627.

22 M. Wang, Y. W. Yang, L. C. Han, F. Xu and F. Li, *J. Cell. Physiol.*, 2020, **235**, 4070–4081.

23 B. Kim, S. L. Stephen, A. M. Hanby, K. Horgan, S. L. Perry, J. Richardson, E. A. Roundhill, E. M. A. Valleley, E. T. Verghese, B. J. Williams, J. L. Thorne and T. A. Hughes, *BMC Cancer*, 2015, **15**, 634.

24 D. Polcari, J. A. Hernandez-Castro, K. Li, M. Geissler and J. Mauzeroll, *Anal. Chem.*, 2017, **89**, 8988–8994.

25 A. Krawczenko, A. Bielawska-Pohl, K. Wojtowicz, R. Jura, M. Paprocka, E. Wojdat, U. Kozlowska, A. Klimczak, C. Grillon, C. Kieda and D. Dus, *PLoS One*, 2017, **12**, e0172371.

26 S. Kuss, D. Polcari, M. Geissler, D. Brassard and J. Mauzeroll, *Proc. Natl. Acad. Sci. U. S. A.*, 2013, **110**, 9249–9254.

27 J. X. Lang, Y. B. Li, Z. Y. Ye, Y. W. Yang, F. Xu, G. Y. Huang, J. J. Zhang and F. Li, *Anal. Chem.*, 2021, **93**, 5797–5804.

28 Y. B. Li, J. X. Lang, Z. Y. Ye, M. Wang, Y. W. Yang, X. J. Guo, J. Zhuang, J. J. Zhang, F. Xu and F. Li, *Anal. Chem.*, 2020, **92**, 4771–4779.

29 D. Polcari, P. Dauphin-Ducharme and J. Mauzeroll, *Chem. Rev.*, 2016, **116**, 13234–13278.

30 S. Rapino, R. Marcu, A. Bigi, A. Solda, M. Marcaccio, F. Paolucci, P. G. Pelicci and M. Giorgio, *Electrochim. Acta*, 2015, **179**, 65–73.

31 Y. Matsumae, Y. Takahashi, K. Ino, H. Shiku and T. Matsue, *Anal. Chim. Acta*, 2014, **842**, 20–26.

32 J. J. Zhang, T. Zhu, J. X. Lang, W. X. Fu and F. Li, *Curr. Opin. Electrochem.*, 2020, **22**, 178–185.

33 C. X. Cai, B. Liu, M. V. Mirkin, H. A. Frank and J. F. Rusling, *Anal. Chem.*, 2002, **74**, 114–119.

34 S. Kuss, D. Trinh and J. Mauzeroll, *Anal. Chem.*, 2015, **87**, 8102–8106.

35 M. S. M. Li, F. P. Filice, J. D. Henderson and Z. F. Ding, *J. Phys. Chem. C*, 2016, **120**, 6094–6103.

36 T. M. Welle, K. Alanis, M. L. Colombo, J. V. Sweedler and M. Shen, *Chem. Sci.*, 2018, **9**, 4937–4941.

37 Z. J. Zhao, X. Y. Gao, J. C. Zeng, S. L. Zhang, X. M. Meng, Y. J. Shen and X. H. Sheng, *J. Phys. Chem. B*, 2020, **124**, 9803–9811.

38 S. Kuss, R. Cornut, I. Beaulieu, M. A. Mezour, B. Annabi and J. Mauzeroll, *Bioelectrochemistry*, 2011, **82**, 29–37.

39 M. Plodinec, M. Loparic, C. A. Monnier, E. C. Obermann, R. Zanetti-Dallenbach, P. Oertle, J. T. Hyotyla, U. Aebi, M. Bentires-Alj, R. Y. Lim and C. A. Schoenenberger, *Nat. Nanotechnol.*, 2012, **7**, 757–765.

40 N. F. Boyd, H. Guo, L. J. Martin, L. Sun, J. Stone, E. Fishell, R. A. Jong, G. Hislop, A. Chiarelli, S. Minkin and M. J. Yaffe, *N. Engl. J. Med.*, 2007, **356**, 227–236.

41 A. Evans, P. Whelehan, K. Thomson, K. Brauer, L. Jordan, C. Purdie, D. McLean, L. Baker, S. Vinnicombe and A. Thompson, *Br. J. Cancer*, 2012, **107**, 224–229.

42 L. J. Martin and N. F. Boyd, *Breast Cancer Res.*, 2008, **10**, 201.

43 D. T. Butcher, T. Alliston and V. M. Weaver, *Nat. Rev. Cancer*, 2009, **9**, 108–122.

44 N. Ballatori, S. M. Krance, R. Marchan and C. L. Hammond, *Mol. Aspects Med.*, 2009, **30**, 13–28.

45 F. Baltes, V. Pfeifer, K. Silbermann, J. Caspers, K. Wantoch von Rekowski, M. Schlesinger and G. Bendas, *Biochim. Biophys. Acta, Mol. Cell Res.*, 2020, **1867**, 118663.

46 D. P. Olson, B. J. Taylor and S. P. Ivy, *Cytometry*, 2001, **46**, 105–113.

47 J. W. Kok, K. Klappe and I. Hummel, *Adv. Biol.*, 2014, **2014**, 105898.

48 B. Trappmann, J. E. Gautrot, J. T. Connelly, D. G. Strange, Y. Li, M. L. Oyen, M. A. Cohen Stuart, H. Boehm, B. Li, V. Vogel, J. P. Spatz, F. M. Watt and W. T. Huck, *Nat. Mater.*, 2012, **11**, 642–649.

49 L. Groth-Pedersen, M. S. Ostenfeld, M. Hoyer-Hansen, J. Nylandsted and M. Jaattela, *Cancer Res.*, 2007, **67**, 2217–2225.

50 F. Zeng, R. J. Ju, L. Liu, H. J. Xie, L. M. Mu and W. L. Lu, *Pharmacology*, 2018, **101**, 43–53.

51 N. Ballatori, C. L. Hammond, J. B. Cunningham, S. M. Krance and R. Marchan, *Toxicol. Appl. Pharmacol.*, 2005, **204**, 238–255.

52 D. W. Loe, R. G. Deeley and S. P. C. Cole, *Cancer Res.*, 1998, **58**, 5130.

53 T. A. Theodossiou, M. Ali, M. Grigalavicius, B. Grallert, P. Dillard, K. O. Schink, C. E. Olsen, S. Walchli, E. M. Inderberg, A. Kubin, Q. Peng and K. Berg, *npj Breast Cancer*, 2019, **5**, 13.